ELSEVIER

Journal of Nuclear Materials 307–311 (2002) 322–326

journal of nuclear materials

www.elsevier.com/locate/jnucmat

The primary origin of dose rate effects on microstructural evolution of austenitic alloys during neutron irradiation

T. Okita [a,*], T. Sato [a], N. Sekimura [a], F.A. Garner [b], L.R. Greenwood [b]

[a] *Department of Quantum Engineering and Systems Science, The University of Tokyo, 7-3-1 Hongo, Bunkyo-ku, Tokyo 113-8656, Japan*
[b] *Pacific Northwest National Laboratory, Richland, WA 99352, USA*

Abstract

The effect of dose rate on neutron-induced microstructural evolution was experimentally estimated. Solution-annealed austenitic model alloys were irradiated at ≃400 °C with fast neutrons at seven different dose rates that vary more than two orders difference in magnitude, and two different doses were achieved at each dose rate. Both cavity nucleation and growth were found to be enhanced at lower dose rate. The net vacancy flux is calculated from the growth rate of cavities that had already nucleated during the first cycle of irradiation and grown during the second cycle. The net vacancy flux was found to be proportional to $(\text{dpa/s})^{1/2}$ up to 28.8 dpa and 8.4×10^{-7} dpa/s. This implies that mutual recombination dominates point defect annihilation in this experiment, even though point defect sinks such as cavities and dislocations were well developed. Thus, mutual recombination is thought to be the primary origin of the effect of dose rate on microstructural evolution.

1. Introduction

Blanket structural component materials in fusion reactors are expected to be exposed for long periods to neutron spectra generated by 14 MeV neutrons, often at dose rates lower than that characteristic of fast reactors. Accelerated irradiation testing conducted at high dose rates in fission reactors is one of the ways to achieve the same cumulative dose levels as required for fusion conditions. However, it is known that dose rates strongly affect microstructural evolution [1–5] and resultant macroscopic property changes [5–7]. It is therefore very important to evaluate the effect of dose rate on microstructural evolution and to develop models incorporating dose rate effects allowing assessments of irradiation performance of fusion materials.

The objective of this study is to experimentally clarify the primary origin of the effect of dose rate on microstructural evolution. Several solution-annealed austenitic alloys were irradiated at actively controlled temperatures with fast neutrons at seven different dose rates over a wide range of dose rate, and showed a very strong influence of dose rate on the transient regime of swelling [5]. The results of further microstructural examination of one alloy are presented in this paper.

2. Experimental procedure

Relatively pure Fe–15Cr–16Ni (at.%) with no added solute was prepared by arc melting from high purity Fe, Ni, and Cr. The ternary alloy was rolled to sheets of 0.25 mm thickness, cut into 3 mm disks and annealed for 30 min at 1050 °C in high vacuum.

Identical specimens are placed in seven different positions of the materials open test assembly (MOTA), ranging from below the core to above the core of the fast flux test facility (FFTF). The first irradiation sequence

* Corresponding author. Tel.: +81-3 5841 6987; fax: +81-3 3818 3455.
E-mail address: okita@qs.t.u-tokyo.ac.jp (T. Okita).

0022-3115/02/$ - see front matter © 2002 Published by Elsevier Science B.V.
PII: S0022-3115(02)01202-3

Table 1
Irradiation conditions in Cycles 11 and 12

Dose rate (dpa/s)		Dose (dpa)		Temperature (°C)	
#11	#12	#11	#11 and #12	#11	#12
1.7×10^{-6}	1.4×10^{-6}	43.8	67.8	427	408
7.8×10^{-7}[a]	9.5×10^{-7}	20.0[a]	32.4	390	387
5.4×10^{-7}	8.4×10^{-7}	14.0	28.8	430	424
3.1×10^{-7}[b]	3.0×10^{-7}	8.05[b]	11.1	411	410
9.1×10^{-8}	2.1×10^{-7}	2.36	6.36	430	431
2.7×10^{-8}	6.6×10^{-8}	0.71	1.87	434	437
8.9×10^{-9}	2.2×10^{-8}	0.23	0.61	436	444

[a] 6.0×10^{-7} dpa/s and 15.6 dpa for two cycle irradiation specimens.
[b] 2.2×10^{-7} dpa/s and 5.69 dpa for two cycle irradiation specimens.

occurred in Cycle 11 of MOTA-2A for 2.58×10^7 s, and a subset of specimens was then removed. Other identical specimens continued in Cycle 12 of MOTA-2B for 1.71×10^7 s. The dose rates ranged from 8.9×10^{-9} to 1.7×10^{-6} dpa/s. The dose levels varied from 0.23 to 43.8 dpa in Cycle 11 and 0.38 to 24.0 dpa in Cycle 12. Table 1 summarizes the irradiation conditions. The microstructural evolution in these specimens was examined using a transmission electron microscope operated at 200 kV.

3. Results

Fig. 1 shows the cavity density as a function of the cumulative dose. The cavity density increases with dose at all dose rates from 8.9×10^{-9} to 1.7×10^{-6} dpa/s. However, both the absolute value and the rate of increase in cavity density are higher at lower dose rates, indicating that lower dose rates enhance cavity nucleation.

Fig. 2 shows a comparison of cavity size distributions for a lower dose rate of 1.5×10^{-7} dpa/s and a higher dose rate of 3.1×10^{-7} dpa/s, both at a cumulative dose level of $\simeq$7 dpa. Cavities with diameters higher than 35 nm can be observed only at the lower dose rate, indicating that cavity growth is also enhanced at low dose rate. It is also notable that a higher density of small cavities with a diameter less than 10 nm can be observed at the lower dose rate, indicating continuous operation of cavity nucleation. Simultaneous enhancement of both cavity nucleation and growth therefore causes accelerated swelling at lower dose rates, as shown in Fig. 3. Note that the swelling data in Fig. 3(a) were derived from microscopy observation below 10% swelling, and from immersion density measurement above 10%, as presented earlier [5]. Microscopy at large swelling levels usually leads to significant intersection and attack of voids near specimen surfaces, and thus an underestimate of swelling compared to density changes, as shown in Fig. 3(b).

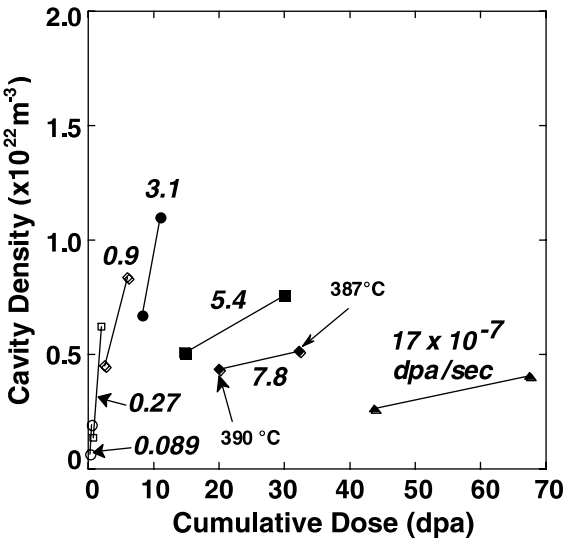

Fig. 1. Cavity densities of Fe–15Cr–16Ni irradiated over a wide range of dose rates as a function of cumulative dose. The dose rates in Cycle 11 are noted in the figure.

Note in Fig. 3(a) that this alloy attains the characteristic steady state swelling rate of $\simeq$1% dpa^{-1} [8,9], and this post-transient swelling rate does not appear to be affected by the dose rate. The transient regime of swelling varied from $<$1 to $\simeq$60 dpa when the dose rate varied over more than two orders of magnitude. The control temperatures of the seven capsules varied from 387 to 444 °C and may have influenced the swelling behavior somewhat. At a fixed dose rate, higher temperature is known to yield higher swelling based on a previous study in this experimental series by Sekimura et al. that showed the peak swelling temperature of this alloy at 1.7×10^{-6} dpa/s to lie at $\simeq$500 °C [10,11]. However, as shown in Fig. 4(a), the incubation dose of swelling at lower dose rate and lower temperature is shorter than that at higher temperature and higher dose rate. This indicates that the dose rate is more important that the variation of irradiation temperature. Fig. 4(b)

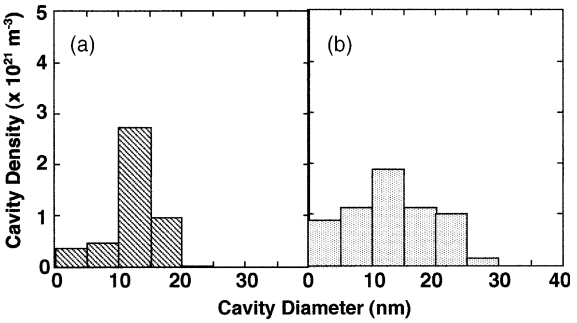

Fig. 2. Comparison of cavity size distribution at similar cumulative dose levels: (a) higher dose rate, one cycle of irradiation in Cycle 11, 8.05 dpa, 3.1×10^{-7} dpa/s at 411 °C; (b) lower dose rate, two cycles of irradiation in Cycles 11 and 12, 2.36 dpa, at 9.1×10^{-8} dpa/s and 430 °C in Cycle 11, and 4.0 dpa at 1.5×10^{-7} dpa/s and 431 °C in Cycle 12, with a cumulative dose of 6.36 dpa.

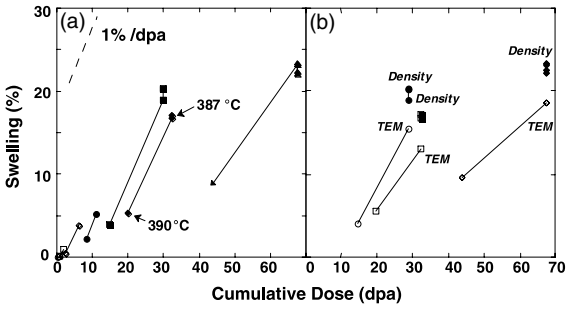

Fig. 3. Swelling over a wide range of dose rates as a function of cumulative dose. (a) Swelling determined by microscopy and density, as originally shown in Ref. [5]. (b) Comparison of swelling between microscopy observation and immersion density measurement at swelling levels >10%. Note that swelling by density is larger than that by microscopy.

shows the swelling as a function of cumulative dose for different dose rates at a very limited temperature range of (437 ± 7) °C. Clearly shown is the strong enhancement of swelling at lower dose rate.

4. Discussion

Microstructural observation shows that cavities in this ternary alloy are homogeneously distributed in the matrix at every irradiation condition, implying that the point defect flux is homogeneous throughout the matrix.

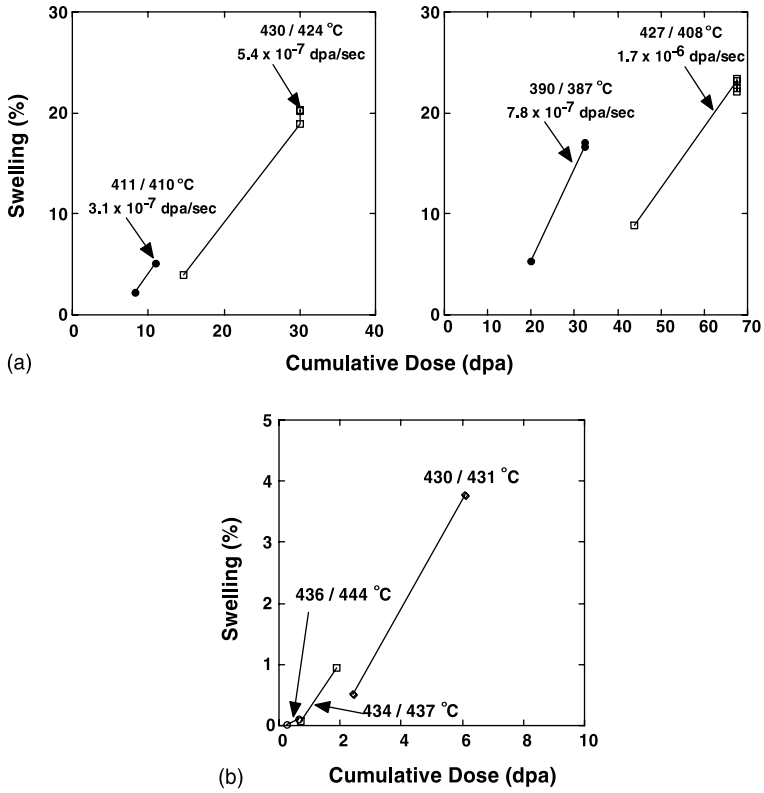

Fig. 4. Comparisons of swelling as a function of cumulative dose. These figures show that dose rate differences affect swelling behavior more strongly than irradiation temperature.

In the following analysis larger cavities observed after two cycles are assumed to have nucleated and started to grow in the Cycle-11 stage of irradiation, while smaller cavities nucleated during Cycle-12 and grew during the remainder of Cycle-12. Cavities observed after the second cycle of irradiation can therefore be divided into the following two categories: 'earlier cavities' that nucleated during the first cycle of irradiation, and 'recent cavities' that nucleated during the second cycle. Fig. 5 shows one example of the cavity size distribution divided into earlier and recent cavities. When the diameters are plotted of earlier cavities, which determine the largest portion of the swelling, it is clearly shown in Fig. 6 that cavity growth is enhanced at low dose rates.

Employing the rate equation approach [12–14], the change of cavity radius is written as follows:

$$\frac{dr}{dt} = \frac{1}{r}(Z_{vv}D_vC_v - Z_{vi}D_iC_v), \quad (1)$$

where r is the cavity radius, D_v and D_i is the diffusion efficiency of vacancies (v) and interstitials (i), respectively, and C_v and C_i is the point defect concentration of vacancies (v) and interstitials (i), respectively, Z_{vv} and Z_{vi} is the bias factor of cavities for vacancies (v) and interstitials (i) respectively.

From Eq. (1) the difference between vacancy and interstitial flux, i.e. the net vacancy flux, is written as Eq. (2):

$$\text{Net vacancy flux} = \bar{r}\frac{dr}{dt}, \quad (2)$$

where $\bar{r}$ is the average radius of earlier cavities during the second cycle of irradiation. Fig. 7 shows the calculated dose rate dependence of the net vacancy flux from the growth rate of earlier cavities. The net vacancy flux is found to be proportional to $(\text{dpa/s})^{1/2}$ up to 28.8 dpa and 8.4×10^{-7} dpa/s. It is known that the point defect concentrations are proportional to $(\text{dpa/s})^{1/2}$ in the recombination-dominant regime [12–17]. This indicates that mutual recombination appears to dominate point defect annihilation up to 30 dpa, even though in this experiment, the point defect sink population is well developed, with the dislocation sink strength as high as 7.11×10^{14} m^{-2} and the cavity sink strength as high as 1.47×10^{15} m^{-2} [5,7] (although the increase rates of these populations are strongly dependent on dose rate [5]).

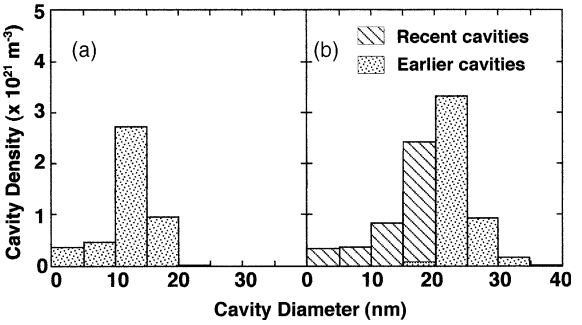

Fig. 5. Dose dependence of cavity size distribution at a fixed dose rate. Note that the density of earlier cavities is the same as that observed after one cycle irradiation: (a) one cycle irradiation to 2.36 dpa at 430 °C and (b) two cycle irradiation to 6.36 dpa at 430/431 °C.

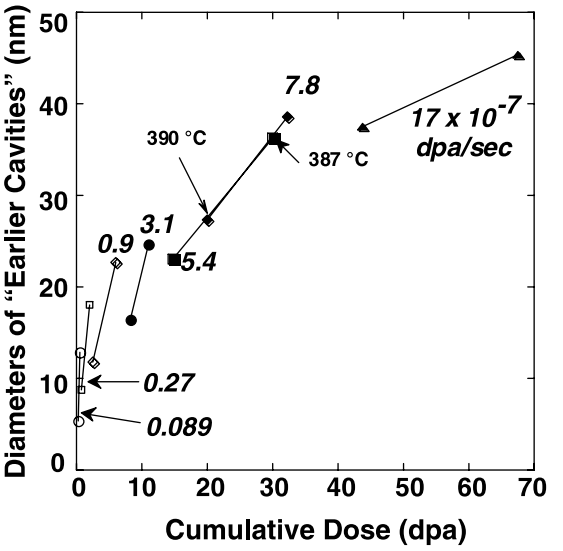

Fig. 6. The diameters of earlier cavities as a function of cumulative dose.

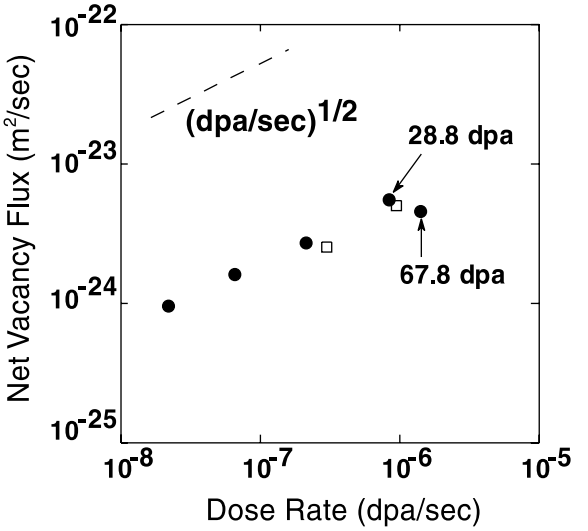

Fig. 7. Dose rate dependence of the net vacancy flux. Circles show that dose rate dependence of specimens irradiated for two cycles is essentially the same as that of one cycle (squares). Note that below 30 dpa and 8.4×10^{-7} dpa/s, the net vacancy flux is proportional to $(\text{dpa/s})^{1/2}$.

If mutual recombination were expected to occur only when the distance between one interstitial and a vacancy is on the order of the first or second nearest neighbor distance, the fraction of point defects annihilated by mutual recombination would be much smaller. Thus, there must exist some other mechanism of point defect recombination. One possibility may be that the recombination area is much larger, possibly the fifth or sixth nearest neighbor. However, further study is necessary to clarify such a possibility. The validation of such a mechanism of mutual recombination becomes more important at low temperature, because the fraction of point defects annihilated by mutual recombination increases with decreasing irradiation temperature.

At higher dose rates, point defects are generated at higher concentrations, resulting in a higher fraction of point defects annihilating by recombination. One would expect that the fraction of point defects escaping from recombination and being absorbed by sinks to be higher at lower dose rates. However, one would not expect recombination to be equally important throughout the range of dose rates studied. This apparent contradiction may arise from other significant effects of dose rate on microstructural evolution. First, enhanced loop growth with lower loop density is observed at lower dose rates [1–5,7,14], resulting in earlier loop unfaulting and an enhanced rate of network dislocation formation [5,7]. It was also shown that the incubation dose of swelling is strongly related to the dose required to form network dislocations [5,18,19].

5. Summary

Solution-annealed austenitic alloys were irradiated at $\simeq$400 °C over a wide range of dose rates, and the effect of dose rate on microstructural evolution was estimated. The net vacancy flux calculated from the cavity growth rate was found to be proportional to $(\text{dpa/s})^{1/2}$ up to 30 dpa. This indicates that the fraction of point defects annihilated by mutual recombination is rather large. Thus, the primary origin of the dose rate effect on microstructural evolution at $\simeq$400 °C lies in the domination of point defect annihilation by recombination and the consequent influence on dislocation and cavity nucleation. In the development of models describing the results of long-term irradiation, it is essential to incorporate the mutual recombination mechanism into the model.

Acknowledgements

This work was supported by Monbusho, the Japanese Ministry of Education, Science and Culture under the FFTF–MOTA collaboration and the JUPITER program (Japan–USA Program for Irradiation Testing for Fusion Research), and the US Department of Energy, Office of Fusion Energy, under Contract DE-AC06-76RLO 1830 at Pacific Northwest National Laboratory, and by the Lawrence Livermore National Laboratory under contract no. W-7405-ENG-48 with the DOE. Additional financial support for T. Okita was provided by Nuclear Fuel Industries, Ltd. The authors are pleased to acknowledge the contributions of PNNL employees Ruby Ermi and Elaine Dieffenbacher for specimen retrieval and preparation.

References

[1] T. Okita, T. Kamada, N. Sekimura, J. Nucl. Mater. 283–287 (2000) 220.
[2] T. Okita, N. Sekimura, T. Iwai, F.A. Garner, Proceedings of 10th International Symposium on Environmental Degradation of Materials in Nuclear Power Systems – Water Reactors, 2001, on CD with no page numbers.
[3] M. Kiritani, J. Nucl. Mater. 169 (1989) 89.
[4] T. Muroga, H. Watanabe, N. Yoshida, J. Nucl. Mater. 174 (1990) 282.
[5] T. Okita, N. Sekimura, F.A. Garner, L.R. Greenwood, W.G. Wolfer, Y. Isobe, Proceedings of 10th International Symposium on Environmental Degradation of Materials in Nuclear Power Systems – Water Reactors, 2001, on CD with no page numbers.
[6] F.A. Garner, M.L. Hamilton, D.L. Porter, T.R. Allen, T. Tsutsui, M. Nakajima, T. Kido, T. Ishii, G.M. Bond, B.H. Sencer, in preparation.
[7] T. Okita, T. Sato, N. Sekimura, F.A. Garner, 'The Effect of Dose Rate on Microstructural Evolution in Austenitic Model Alloys Irradiated with Fast Neutrons', Proc. Fourth Pacific Rim Int. Conf. on Advanced Materials and Processing (PRICM4), The Japan Institute of Metals, 2001, p. 1403.
[8] F.A. Garner, 'Irradiation Performance of Cladding and Structural Steels in Liquid Metal Reactors', Materials Science and Technology: A Comprehensive Treatment, VCH, 1994, Vol. 10A, Chapter 6, p. 419.
[9] F.A. Garner, J. Nucl. Mater. 117 (1983) 177.
[10] N. Sekimura, K. Hamada, S. Ishino, J. Nucl. Mater. 179–181 (1991) 542.
[11] N. Sekimura, S. Ishino, ASTM-STP 1175 (1994) 992.
[12] L.K. Mansur, Nucl. Technol. 40 (1978) 5.
[13] Y. Katoh, A. Kohyama, R.E. Stoller, J. Nucl. Mater. 212–215 (1994) 179.
[14] R.E. Stoller, G.R. Odette, J. Nucl. Mater. 131 (1985) 118.
[15] L.K. Mansur, W.A. Coghlan, J. Nucl. Mater. 119 (1983) 1.
[16] H. Watanabe, A. Aoki, H. Murakami, T. Muroga, N. Yoshida, J. Nucl. Mater. 155–157 (1988) 815.
[17] M. Kiritani, N. Yoshida, H. Tanaka, Y. Maehara, J. Phys. Soc. Jpn. 39 (1975) 170.
[18] T. Muroga, F.A. Garner, S. Ohnuki, J. Nucl. Mater. 179–181 (1991) 546.
[19] T. Muroga, F.A. Garner, J.M. McCarthy, N. Yoshida, ASTM-STP 1125 (1992) 1015.